Multiaxial fatigue behavior of AISI 316L subjected to strain-controlled and ratcheting paths

G. Facheris [a], K.G.F. Janssens [a,*], S. Foletti [b]

[a] Laboratory for Nuclear Materials, Nuclear Energy and Safety Research Department, Paul Scherrer Institute, Villigen PSI, Switzerland
[b] Dipartimento di Meccanica, Politecnico di Milano, Milano, Italy

Article history:
Received 27 January 2014
Received in revised form 9 May 2014
Accepted 15 May 2014
Available online 23 May 2014

1. Introduction

The main goal of the current work is to present a detailed experimental analysis of the cyclic deformation behavior and of the fatigue endurance of a AISI 316L stainless steel grade under loading conditions typical for the primary cooling circuit of a light water nuclear reactor. In the last decades, some infamous industrial incidents demonstrated that thermo-mechanical fatigue (TMF) plays a role in the crack initiation and propagation process for this class of components [1]. It has been shown [2] that moving temperature gradients induced by a thermal-shock can cause a local yielding, under certain conditions leading to local ratcheting. A reliable prediction of the number of cycles to failure needs accurate knowledge of the deformation behavior of a material, for which purpose several authors have studied the mechanical response of stainless steels when subjected to ratcheting. Many studies investigate the ratcheting response of stainless steels prescribing a uniaxial, non-symmetric alternate stress history [3–7]. Other authors evaluate the influence of ratcheting for the multiaxial loading case, using stress control for at least one of the two controlled deformation axes [3,7–10]. The fact that these ratcheting experiments are stress-controlled prohibits a direct comparison with strain-controlled LCF tests, as the strain path in either experiment is different. An alternative way to analyze the cyclic ratcheting response for the uniaxial loading case is to use *strain-controlled* ratcheting tests (also known as cyclic tension tests) [11]. In strain-controlled ratcheting experiments the strain path consists of a superposition of a cyclic part, e.g. with a constant strain rate and a fixed amplitude, and a part consisting of a continuously varying mean strain. Few results for this fully strain controlled-approach have been published by Ohno et al. [12], Mizuno et al. [13], Facheris and Janssens [14]. In the current work, the strain-based approach is extended to selected multiaxial ratcheting conditions. According to our knowledge, no reference is available in literature for multiaxial ratcheting experiments performed controlling both the axial and torsional axis of the testing machine in strain.

An improved constitutive description of the mechanical behavior of stainless steels is essential for the development of advanced fatigue criteria to enhance the accuracy of fatigue life prediction, especially in this class of materials, characterized by a strong deformation history dependency under multiaxial loading and ratcheting. The evident drawbacks of the classical fatigue models when dealing with multiaxiality, led researchers to develop critical plane criteria [15] considering the accumulation of fatigue damage to occur in a specific material plane.

Among these criteria, Smith–Watson–Topper [16], and Fatemi–Socie [17] are commonly used strain-based fatigue models considering the effects of mean stress and additional hardening to enhance the accuracy of the fatigue life predictions. The first one is suitable for material showing a normal cracking mode, whereas

* Corresponding author.
E-mail address: koen.janssens@psi.ch (K.G.F. Janssens).

the second one is ideal for shear cracking. Other approaches consist of associating the damage accumulation with the energy absorbed during the cyclic deformation [18,19]. As an example, the Jiang [20] fatigue damage criterion, not requiring any cycle counting, provides a way to make fatigue life predictions when complex loading paths are imposed. Further examples of these stress–strain- and energy-based fatigue criteria, proposed in the past few years, further improve the accuracy of the fatigue life predictions under complex loading conditions including multiaxial loading paths and ratcheting [21–23].

In the first part of the article, the investigated material is characterized and the testing equipment is described together with the comprehensive list of the performed experiments. The three selected fatigue criteria used to assess the life endurance are briefly described.

The second part of the current work consists in the presentation of the room temperature material response of AISI 316L under uniaxial, torsional and a selection of multiaxial low cycle fatigue (LCF) conditions involving ratcheting. It is well known [3,7,13,24] that, even at room temperature, AISI 316L shows a viscoplastic mechanical behavior, meaning that the loading rate influences the material response under LCF and ratcheting loading conditions. This time-dependency is not taken into account in the current work and all tests have been performed imposing an equal strain rate.

In the third part of the article, a detailed analysis of the experimentally observed fatigue lives is presented together with a discussion on the effect of ratcheting and of the imposed loading path. Finally, an evaluation of the performance of three advanced critical plane fatigue criteria in predicting the life of the specimens under the prescribed loading conditions is reported.

2. Material characterization

A 20 mm thick hot rolled plate made of stainless steel grade AISI 316L has been used to fabricate two, geometrically different kinds of fatigue specimens, suitable for uniaxial and multiaxial (tension–torsion) experiments. The chemical composition for the investigated material is listed in Table 1. The manufacturing sequences consist of: hot working, solution annealing (at 1050–1080 °C), quenching in water, pickling and grinding. The plate material, in the as received condition, is characterized by a precipitate free austenitic matrix microstructure with some inclusions, annealing twins and an average grain size of about 50 μm. The basic mechanical properties of the investigated AISI 316L are summarized in Table 2.

Parallelepipeds with a 20 mm wide, square cross section have been extracted from the plate along the rolling direction. From these parallelepipeds are then manufactured:

- Specimens with a diameter of 8 mm for performing uniaxial tests according to the standard ASTM E606-12 [25] (see Fig. 1a).
- Hollow samples with an outer diameter of 16 mm and an inner diameter of 13 mm for performing torsional/multiaxial tests according to the standard ASTM E2207-08 [26] (see Fig. 1b). The resulting wall thickness of 1.50 mm is a trade-off limiting unwanted buckling effects and minimizing the radial variation of the shear stress.

3. Experiments

3.1. Uniaxial experimental setup

The uniaxial experiments have been executed using a 250 kN uniaxial Schenk Hydropuls fatigue bench and controlling the machine in strain by a clip-on extensometer having an initial gage of 20 mm and a displacement range of ±1.25 mm. All the tests have been performed at room temperature. Whereas LCF tests have been carried out according to the ASTM norm [25], no standard is available for ratcheting experiments.

The LCF tests have been performed imposing a strain path in axial direction (see Fig. 2a) with ramp waveform with three different strain amplitudes (0.40%, 0.65% and 1.00%) and changing the cycling period in order to obtain a constant strain rate over all the experiments (equal to 0.32%/s).

While ratcheting tests are commonly performed under stress control, only few literature references on strain-controlled ratcheting experiments are available [12–14]. In the current work, strain-controlled instead of stress-controlled ratcheting tests are performed to obtain a directly comparable strain path in all experiments. The strain-controlled ratcheting experiments consist of a superposition of a constant amplitude ramp waveform and a continuously increasing mean strain. The ratcheting rate is characterized by means of the ratcheting step ξ, which is defined as the per-cycle accumulation of the mean strain. When the mean strain reaches the limit of 5%, the limit of the extensometer range is reached, and the mean strain is kept constant during the remainder of the experiment till failure. Among the ratcheting tests reported in a previous study [14], only the experiment performed using a strain amplitude of 0.65% and a ratcheting step of +0.1%/cycle is considered in the current work.

3.2. Torsional and multiaxial experimental setup

The torsional and multiaxial experiments are executed using a tension–torsion servo-hydraulic testing system MTS 809 having a capacity of 250 kN axial force and of 2500 Nm torque. The tests are carried out controlling in strain the torsional and/or the tension axes by means of a biaxial extensometer having an initial gage of 25 mm, a displacement range limited to ±2.50 mm and a rotation range of maximum ±5.0°. No internal pressure is imposed and all experiments are performed at room temperature.

Table 1
Standard designations and chemical composition of the investigated austenitic stainless steel (weight percentages).

ASME SA-312/SA312M	SN EN 10216-5	C	Si	Mn	P	S	Cr	Ni	Mo	N
316L	X2CrNiMo17-3	0.024	0.46	1.59	0.039	0.001	17.51	12.53	2.55	0.0859

Table 2
Basic mechanical properties of the investigated austenitic stainless steel.

ASME SA-312/SA312M	yield stress $R_{p0.2}$ (MPa)	ultimate tensile strength R_m (MPa)	elongation A_{50} (%)
316L	265 ± 5	585 ± 5	60 ± 2

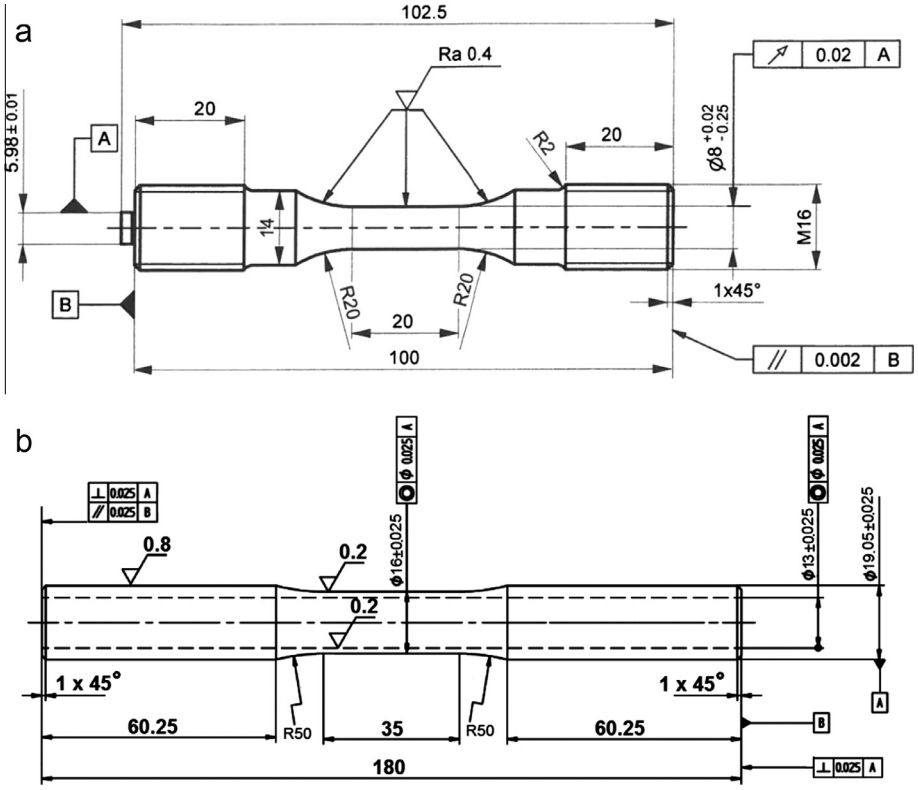

Fig. 1. Geometry of specimens used for uniaxial (a) and torsional/multiaxial (b) fatigue experiments.

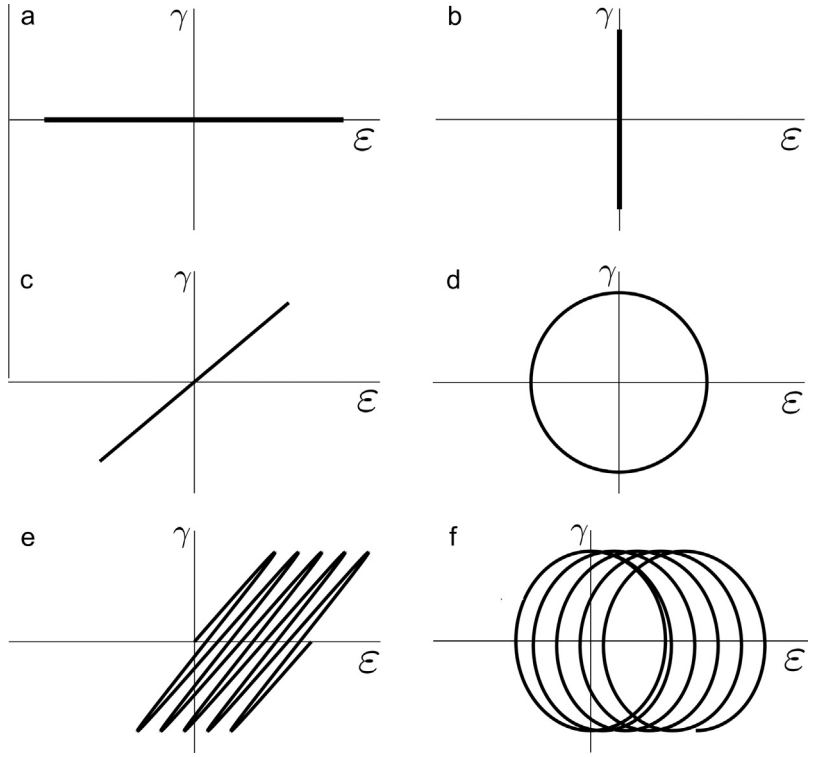

Fig. 2. Imposed strain paths: (a) uniaxial, (b) torsional, (c) multiaxial proportional, (d) multiaxial non-proportional, (e) multiaxial proportional ratcheting, and (f) multiaxial non-proportional ratcheting.

Torsional and multiaxial LCF tests have been carried out according to the ASTM regulations [26]. No standard is available for the execution of ratcheting experiments. Torsional LCF experiments are performed imposing a strain path in shear direction (see Fig. 2b) with three different, equivalent strain amplitude levels (i.g. 0.40%, 0.65% and 1.00%) and with the same cycling periods

as in the uniaxial tests. The equivalent strain ε^{eq} is defined as a combination of strain in axial ε and in shear direction γ computed by means of Eq. (1) consisting in an adaptation of the von Mises criterion for strains in which the deformation is assumed to be isochoric.

$$\varepsilon^{eq} = \sqrt{\varepsilon^2 + \frac{1}{3}\gamma^2} \tag{1}$$

Two types of multiaxial LCF experiments are carried out controlling the strain simultaneously in axial and in shear direction, and imposing two different strain paths. In the first case, the experiment is 'proportional' without phase shift between the axial and the shear loading histories, and keeping the strain component amplitudes equivalent (see Fig. 2c). In the second case, a phase shift with magnitude $\pi/2$ is imposed, defining the strain path to be 'non-proportional' and resulting in the circular path that is shown in Fig. 2d. These tests are carried out for an equivalent strain amplitude level equal to 0.65%, using the same cycling period as in the corresponding uniaxial experiment.

The multiaxial ratcheting tests consist of two strain-controlled experiments in which the LCF loading paths are overlapped to a continuously increasing mean strain in axial direction (see Fig. 2e and f). These tests are carried out for an equivalent strain amplitude level equal to 0.65% and a constant ratcheting step of +0.1%/cycle. As for the uniaxial ratcheting tests, when the axial mean strain reaches a value of 5%, the axial mean strain is kept constant and the experiment is continued until failure.

The relation between the shear stress τ and the measured torque M is given by Eq. (2) assuming the stress to be linearly distributed along the specimen thickness. A detailed discussion on the validity of this assumption is reported in Section 5.

$$M = \int_A \tau \cdot r \cdot dA = \frac{\tau}{r}\int_A r^2 \cdot dA = \frac{\tau \cdot J_p}{r} \tag{2}$$

For a hollow sample, the shear stress on the external surface of the specimen is computed by means of Eq. (3), expressing the polar moment of inertia J_p as a function of the internal D_{int} and of the external diameter D_{ext}.

$$\tau(D_{ext}) = \frac{M \cdot D_{ext}/2}{\pi/32(D_{ext}^4 - D_{int}^4)} \tag{3}$$

3.3. Test designation

The name of each test is coded to allow the reader to identify the type of the experiment (e.g. uniAXial, TOrsional, Multiaxial Proportional or Multiaxial Non-proportional and 'L' for LCF or 'R' for ratcheting). The information regarding the imposed equivalent strain amplitude is indicated in the next position of the experiment name. For ratcheting tests, the information about the ratcheting step is given at the end of the name ('P' stands for positive ratcheting). As an example, MN-R-065-P10 refers to a multiaxial, non-proportional ratcheting test performed with an equivalent strain amplitude of 0.65% and a positive ratcheting step of 0.1%/cycle. The complete list of experiments with the corresponding test parameters is summarized in Table 3.

4. Criteria for fatigue assessment

Three critical plane fatigue criteria have been used in the current study to predict the number of cycles to failure: the Smith–Watson–Topper, the Fatemi–Socie and the Jiang model. These models have been selected for their recognized capability to provide reliable fatigue life predictions for the investigated class of material when subjected to uniaxial and multiaxial loading conditions.

4.1. Smith–Watson–Topper

The original Smith–Watson–Topper [16] (SWT) criterion (see Eq. (4)) consists in a modification of the Coffin–Manson [27,28] law improving the accuracy of life predictions under axial tension–compression loading conditions taking into account the effect of a non-zero mean stress.

$$\begin{aligned} P_{SWT} &= \sigma_{max}\varepsilon_{ampl} = \frac{\sigma_f'^2}{E}\cdot(2N_f)^{2b} + \sigma_f'\varepsilon_f'\cdot(2N_f)^{b+c} \\ &= A_1\cdot(2N_f)^{a_1} + A_2\cdot(2N_f)^{a_2} \end{aligned} \tag{4}$$

Considering only the stresses and the strains occurring in the critical plane defined as the plane of maximum normal strain range, it is possible to modify the criterion as shown in Eq. (5) allowing its use in a multiaxial loading context.

$$P_{SWT} = \sigma_{c,max}\varepsilon_{c,ampl} = A_1\cdot(2N_f)^{a_1} + A_2\cdot(2N_f)^{a_2} \tag{5}$$

$\sigma_{c,max}$ and $\varepsilon_{c,ampl}$ are the maximum normal stress and the normal strain amplitude on the critical plane. The parameters A_1, a_1, A_2 and a_2 are calibrated fitting the room temperature ASME-III mean air curve for AISI 316L [29] as shown by Janssens et al. [30] and their values are reported in Table 4.

4.2. Fatemi–Socie

The Fatemi–Socie [17] (FS) criterion consists in a critical plane shear-strain based multiaxial criterion (see Eq. (6)).

$$P_{FS} = \gamma_{c,ampl}\cdot\left(1 + K\frac{\sigma_{c,max}}{\sigma_y}\right) = \frac{\tau_f'}{G}\cdot(2N_f)^{b^*} + \gamma_f'\cdot(2N_f)^{c^*} \tag{6}$$

Table 3
Summary of the testing parameters used to perform uniaxial, torsional and multiaxial strain-controlled LCF and ratcheting experiments at room temperature.

Test designation	Typology	Loading path	ε_{ampl} (%)	γ_{ampl} (%)	ε^{eq}_{ampl} (%)	ε_{mean} (%)	ξ (%/cycle)
AX-L-040	LCF	axial	0.40	0	0.40	0	0
AX-L-065	LCF	axial	0.65	0	0.65	0	0
AX-L-100	LCF	axial	1.00	0	1.00	0	0
AX-R-065-P10	RAT	axial	0.65	0	0.65	0–5	+0.10
TO-L-040	LCF	torsional	0	$0.40\sqrt{3}$	0.40	0	0
TO-L-065	LCF	torsional	0	$0.65\sqrt{3}$	0.65	0	0
TO-L-100	LCF	torsional	0	$1.00\sqrt{3}$	1.00	0	0
MP-L-065	LCF	multiax. prop.	$0.65\sqrt{2}/2$	$0.65\sqrt{6}/2$	0.65	0	0
MN-L-065	LCF	multiax. non-prop.	0.65	$0.65\sqrt{3}$	0.65	0	0
MP-R-065-P10	RAT	multiax. prop.	$0.65\sqrt{2}/2$	$0.65\sqrt{6}/2$	0.65	0–5	+0.10
MN-R-065-P10	RAT	multiax. non-prop.	0.65	$0.65\sqrt{3}$	0.65	0–5	+0.10

Table 4
Material constants used in the fatigue criteria.

SWT	FS γ_{ampl}^{max}	FS P_{FS}^{max}	Jiang
A_1 = 500	K = 0.65	K = 1.00	a = 0.5
a_1 = −0.7	σ_y = 265 MPa	σ_y = 265 MPa	D_0 = 12,000 MPa
A_2 = 0.6	G = 73,000 MPa	G = 73,000 MPa	σ_0 = 180 MPa
a_2 = −0.02	τ_f' = 348.6 MPa	τ_f' = 348.6 MPa	σ_f = 820 MPa
	γ_f' = 0.5289	γ_f' = 0.5289	m = 1.8
	b^* = −0.0434	b^* = −0.1365	n = 0.015
	c^* = −0.4784	c^* = −0.4237	

$\sigma_{c,max}$ and $\gamma_{c,ampl}$ are the maximum normal stress and the shear strain amplitude on the critical plane.

σ_y is the yield stress of AISI 316L, K is a material constant and the right hand side term of Eq. (6) represents the torsional Coffin-Manson curve. Depending on the adopted definition for the critical plane, two versions of Fatemi–Socie criterion have been implemented. In 'Fatemi–Socie γ_{ampl}^{max}' the critical plane is defined as the plane of maximum shear strain amplitude. In 'Fatemi–Socie P_{FS}^{max}' the critical plane is the material plane in which the parameter P_{FS} is maximum. For the 'γ_{ampl}^{max}' version of the damage criterion, the parameters τ_f', γ_f', b^* and c^* can be fitted to our experimental data (AX-L-xxx and TO-L-xxx), and K is computed following the procedure published by Socie and Marquis [31], i.e. calibrating its value so that the uniaxial and the torsional fatigue data align on a single curve. The same calibration procedure is not valid for the 'P_{FS}^{max}' version of the Fatemi–Socie criterion, since in this case the determination of the critical plane depends on the value attributed to K. To solve this problem an iterative solution method has been implemented, consisting of a repeated sequence of first changing the parameters of the fatigue curve (τ_f', γ_f', b^* and c^*), and second changing K. This sequence is repeated until the alignment of the uniaxial and the torsional fatigue data converge to the same curve. The values of the calibrated parameters are listed in Table 4.

4.3. Jiang

The Jiang [20] model consists of a critical plane, plastic work-based multiaxial criterion combining the energy and the material memory concept. The increment of damage in a material plane is computed using Eq. (7) where σ_{mr} is the material memory stress, σ_0 represents the endurance limit, σ_f is the true fracture stress and dY is the increment of plastic strain energy.

$$dD = \left\langle \frac{\sigma_{mr}}{\sigma_0} - 1 \right\rangle^m \left(1 + \frac{\sigma_c}{\sigma_f}\right) dY \tag{7}$$

The first factor on the right side of Eq. (7) is used to consider the loading sequence effect. This feature is necessary to reproduce the fatigue life reduction effect occurring in certain materials when a sequence of high–low loading is applied instead of an equivalent low–high sequence [32]. To take into account the loading magnitude effect, a memory surface concept is introduced. The evolution for the memory stress σ_{mr} is defined by Eq. (8).

$$d\sigma_{mr} = \sqrt{\frac{3}{2}} H(g) \left\langle \frac{\mathbf{s}}{||\mathbf{s}||} : d\mathbf{s} \right\rangle - n[1 - H(g)](\sigma_{mr} - \sigma_0) dp \tag{8}$$

where $\mathbf{s}$ is the deviatoric stress tensor, $H(x)$ is the Heaviside function, n is a material constant governing the contraction of the memory surface, p is the equivalent accumulated plastic strain and g corresponds to the memory surface for fatigue defined as

$$g = ||\mathbf{s}|| - \sqrt{\frac{2}{3}} \sigma_{mr} \leqslant 0 \tag{9}$$

The increment of plastic strain energy dY is calculated as in Eq. (10) where σ_c is the normal stress and τ_c is the shear stress on the critical plane. $d\varepsilon_c^p$ and $d\gamma_c^p$ represent the plastic strain increment corresponding to σ_c and τ_c respectively.

$$dY = a \cdot \sigma_c \cdot d\varepsilon_c^p + \frac{1 - a}{2} \cdot \tau_c \cdot d\gamma_c^p \tag{10}$$

The value of the endurance limit σ_0 is retrieved from the strain-life curve for fully reversed tension–compression tests. The tensile strength σ_f is determined from a standard tensile experiment. n is derived as described by Jiang [20], i.e. performing uniaxial fatigue tests in a two-step high–low loading sequence and fitting the reduction rate of the cyclic stress amplitude. D_0 corresponds to the average of the damage accumulated by the specimens subjected to three uniaxial LCF tests performed with different strain amplitudes (AX-L-040, AX-L-065, AX-L-100). Finally m and a have been estimated using data corresponding to torsional fatigue tests (TO-L-xxx) and following the procedure explained in detail by Jiang [20]. The values attributed to the parameters of the fatigue criterion are reported in Table 4. Depending on the adopted definition for the critical plane, two versions of Jiang criterion have been implemented. In 'Jiang D^{max}' the critical plane is defined as the plane in which the accumulated fatigue damage D first reaches the critical value D_0. In 'Jiang dD^{max}' the critical plane is defined as the plane in which the damage accumulation increment dD is maximum.

5. Deformation behavior

Data corresponding to uniaxial, torsional and multiaxial tests are analyzed to evaluate the deformation behavior of the AISI 316L. The cyclic evolution of the stiffness and of the yield point cannot be measured for multiaxial non-proportional experiments since, except for the first loading, the mechanical response does not switch between elastic and plastic behavior for all the duration of the test (except for the first loading).

5.1. LCF: Zero-mean strain low cycle fatigue experiments

5.1.1. Elastic and shear modulus

While a fatigue bench is not the ideal equipment to retrieve accurate stiffness measurements, the methodology proposed by Facheris and Janssens [14] is adopted in the current study to get rid of the systematic errors due to the error on the determination of the cross sectional geometry of the sample and/or to small differences in the extensometer positioning. This approach consists in shifting the measured data so that the elastic modulus for the undeformed material, observed at the beginning of the first cycle, is the same value for all the considered experiments, thereby allowing a relative comparison of the measured values. The range of the shift observed in the experiments is indicated in the plots by a vertical line terminated with asterisks.

The apparent elastic modulus E is evaluated for each cycle considering the loading and the unloading traits of the hysteresis loop σ–ε and only a negligible difference between those two values is found during cycling. In an analogous way, the value of the apparent shear modulus G is estimated using the hysteresis loops τ–γ as input. The per-cycle-mean value for the shear and the elastic modulus is plotted as a function of the equivalent accumulated plastic strain (see Fig. 3), evaluated at the beginning of the corresponding hysteresis loop. For uniaxial tests a monotonic reduction of the apparent Young's modulus is observed during cycling (see Fig. 3b). Moreover, imposing a higher strain amplitude level, a faster decreasing of measured stiffness is noticed. Analyzing torsional data, the same qualitative and quantitative behavior (considering a Poisson coefficient of 0.3) is observed for the apparent shear

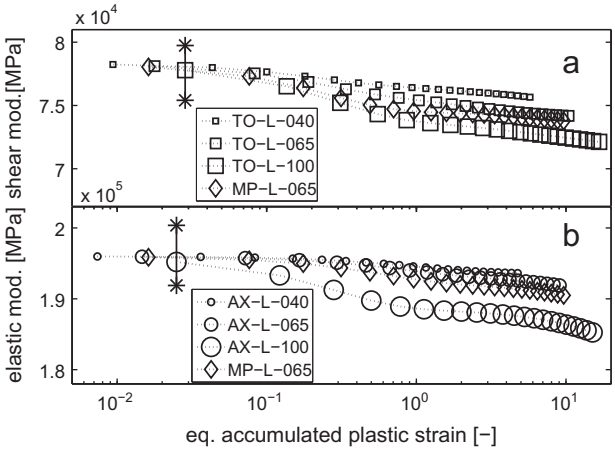

Fig. 3. Shear (a) and elastic modulus (b) versus equivalent accumulated plastic strain for uniaxial, torsional and multiaxial proportional experiments.

modulus (see Fig. 3a). According to Polák et al. [33], the stiffness reduction promoted by cyclic loading is associated with the additional anelastic strain due to bowing out of dislocation segments. Prescribing a higher strain amplitude level, this reduction is accelerated by the enhanced production of new dislocation segments due to dislocation multiplication.

The same analysis is performed for multiaxial proportional tests considering stress and strain measurements in axial and shear direction. The observed reduction for E and G is qualitatively and quantitatively similar to the one reported for uniaxial and torsional experiments performed with the same equivalent strain amplitude level (0.65%).

5.1.2. Yield stress

In austenitic stainless steels, as is AISI 316L, the transition between the elastic and the plastic regime is extremely gradual. For that reason, the determination of the proportionality limit is often problematic since the definition adopted to evaluate the yield may influence the evaluation of the results. While in cyclic plasticity the offset concept is widely used for the definition of the yield stress, no universally accepted threshold value is defined. As commonly recognized, the adoption of the 0.2% offset concept generally used in monotonic tests, is not applicable to LCF data in which this strain value is comparable to the imposed strain amplitude. As reported by Jiang and Zhang [34], the determination of the yield stress using an offset smaller than 0.001% is not possible due to practical limitations linked with the measurement reliability. As a consequence, the offset value is commonly chosen in the range 0.01–0.05%.

In the current work, a study is carried out to show the importance of the selection of this offset value for uniaxial, torsional and multiaxial experiments. Two analyses are performed using two different thresholds: the first similar to the one usually adopted in literature (0.025%) and the second one ten times smaller (0.0025%). To allow a quantitative comparison between data corresponding to uniaxial and torsional experiments, the yield offset thresholds and the yield stresses are referred as the equivalent ones. For the torsional tests, the Von Mises criterion can be simplified and the equivalent yield stress is obtained scaling the yield stress in shear direction τ by a factor of $\sqrt{3}$. In the case of multiaxial tests, the equivalent yield stress is calculated considering both the axial and the shear stress contribution ($\sqrt{\sigma^2 + 3\tau^2}$). For each offset concept, an evaluation of the equivalent yield stress along the loading and unloading trait of the hysteresis loop is performed and only a negligible difference between these two values is found during cycling. The equivalent mean yield stress is then plotted as a function of the accumulated equivalent plastic strain for the two different yield definitions for the uniaxial (Fig. 4a and b), torsional (Fig. 4c and d) and multiaxial proportional experiments (Fig. 4e and f).

Comparing the upper and the lower graphs, one can observe the qualitative difference for uniaxial tests and for data corresponding to torsional experiments. For the highest offset value (e.g. 0.025%), the calculated yield stress is influenced by the strain amplitude and, for the highest amplitude, cyclic hardening is observed instead of softening (see Fig. 4a, c and e). On the other hand, when the lower offset (e.g. 0.0025%) is adopted (see Fig. 4b, d and f), the dependency of the cyclic evolution of the yield stress on the strain amplitude is weaker, though the lower threshold does suffer from more uncertainty. As an additional remark, it is found that the equivalent yield stress is consistently 5–10% higher in torsional tests. The reason for this difference is explained in the next paragraph attributing it to the inaccurate assumption adopted to retrieve the shear stress from the measured torque value.

The current analysis confirms the conclusions reported in a previous study [14], underpinning that the adoption of different yield definitions leads to dissimilar results. This aspect should be carefully considered when a constitutive model is calibrated since the selection of the offset threshold will determine in which measure the mechanical behavior is attributed to isotropic or to kinematic cyclic hardening.

The analysis of the yielding point in multiaxial proportional tests (see Fig. 4e and f) returns yield stress values that for both the considered offset definitions are qualitatively similar and a bit higher than the ones observed in the torsional experiment performed with the same equivalent strain amplitude.

5.1.3. Cyclic hardening/softening

As reported by several authors [3,35–39], stainless steels show a particularly complex mechanical response when subjected to repeated loading. The imposed strain amplitude and loading path are known to quantitatively and qualitatively affect the cycling hardening–softening behavior of AISI 316L.

An effective approach to compare uniaxial and torsional LCF data is to represent the maximum Von Mises equivalent stress evolution as a function of the number of cycles (see Fig. 5). For both testing typologies, AISI 316L shows primary hardening followed by softening and then stabilization. For the experiments with the highest strain amplitude (1.00%), one notices a secondary hardening that is more pronounced in the uniaxial experiment. A careful analysis reveals that, in the first cycles, the measured stress response is 10–15% higher in the torsional tests compared with

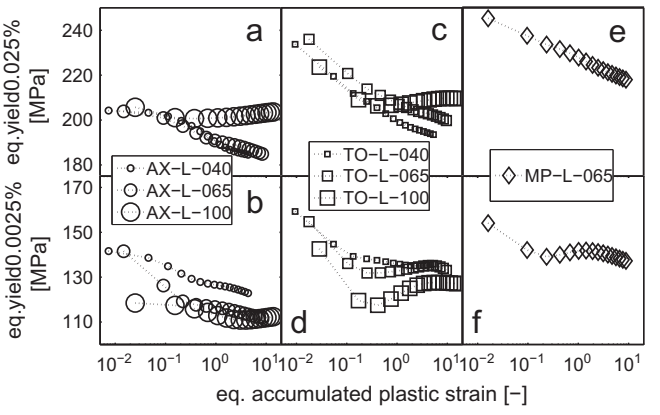

Fig. 4. Equivalent yield stress versus equivalent accumulated plastic strain in uniaxial (a, b) torsional (c, d) and multiaxial proportional (e, f) experiments.

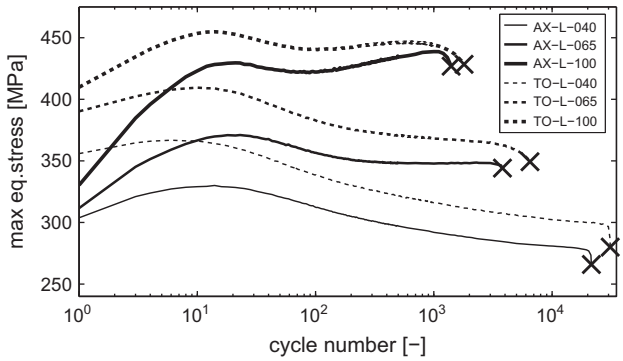

Fig. 5. Maximum equivalent stress versus number of cycles in uniaxial and torsional LCF experiments performed at three different equivalent strain amplitudes.

the uniaxial ones. This difference slowly but not completely fades out during cycling with a rate that is faster in the case of experiments performed with higher equivalent strain amplitudes. This observation is not completely consistent with literature: in the experiments performed by Delobelle [3], Benallal and Marquis [38] and Tanaka et al. [39] the difference between the equivalent response in uniaxial and torsional tests is reported to be negligible.

The difference noticed in the current work is mainly attributed to the experimental error caused by assuming a linear shear stress distribution along the radius of the specimen (see Fig. 6a). It is relatively easy to demonstrate that retrieving the shear stress τ from the measured torque M by means of Eq. (3) (derived from Eq. (2)) leads to inaccurate results when plasticity occurs. In fact, in the case of inelastic deformation, the shear stress distribution is not linear along the radius of the specimen and the ratio τ/r is no longer a constant. To approximately solve this problem, the ASTM norm [26] suggests to assume the shear stress to be uniformly distributed along the thickness of the specimen (see Fig. 6b) and to compute τ by means of Eq. (11).

$$\tau(D_{ext}) = \frac{M}{\pi/16(D_{ext}^2 - D_{int}^2)(D_{ext} + D_{int})} \tag{11}$$

Neither of these assumptions are correct since in reality the shear stress profile is non-linear and changes continuously during loading. To quantify the corresponding error, a set of FEM (Finite Element Method) simulations using an internal variable dependent, Chaboche-type [40] elasto-plastic material description is performed for the three torsional experiments TO-L-xxx. A detailed description concerning the formulation and the calibration of this constitutive model with the capability to reproduce cyclic hardening and the dependency of the latter on the imposed strain amplitude was published elsewhere [41]. The parameters of this constitutive law have been calibrated on a large set of uniaxial LCF and ratcheting tests including the experiments AX-L-xxx and AX-R-065-P10 presented in this article.

The simulated torque M is used as input for Eqs. (3) and (11) to compute the resulting τ. The per-cycle maximum values of τ are then compared to the maximum shear stress extrapolated from a node on the external surface of the specimen (see Fig. 7). As expected, while Eq. (3) overestimates the value of the shear stress on the external surface, Eq. (11) underestimates it. The shear stress computed assuming a uniform distribution of τ is generally more precise than the one calculated postulating a linear distribution. However, it is noticed that, because of the inhomogeneous stress field promoted by the cyclic hardening, the assumption of a uniform stress distribution becomes less and less accurate with the increasing of the number of cycles. Since, these data will be later

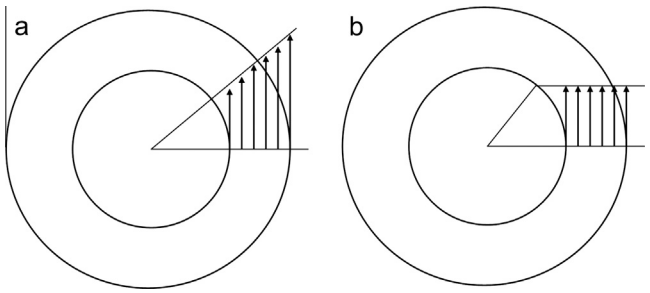

Fig. 6. Linear (a) and uniform (b) shear stress distribution profiles along the thickness of an hollow specimen subjected to torsion.

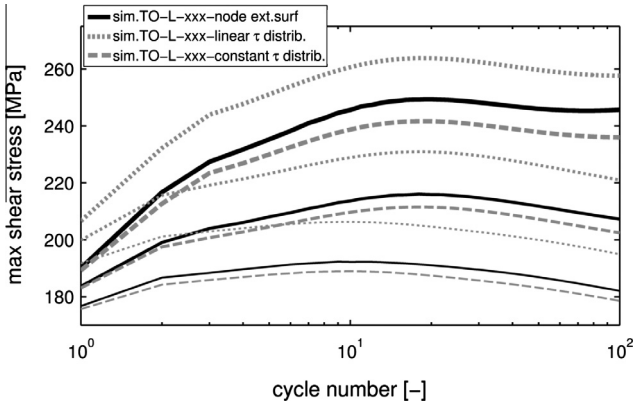

Fig. 7. Maximum shear stress versus number of cycles in simulations of torsional experiments. The shear stress is computed deriving it from the torque value or extrapolating it from one node on the external surface of the specimen.

used as input for damage criteria (see Section 6), in the remainder of the current work we chose to compute τ by means of Eq. (3), hence favoring conservative fatigue life predictions.

For the equivalent strain amplitude level 0.65%, multiaxial proportional and non-proportional LCF tests are performed and the maximum equivalent stress evolution is reported in Fig. 8 together with the corresponding uniaxial and torsional data. According to literature [3,38,39] the stress response measured in the proportional test is nearly identical to the torsional one. On the other hand, in the non-proportional experiment, the activation of multiple slip systems causes, as expected, a considerable additional hardening compared to the proportional test (up to 50–60% higher). As reported by Benallal and Marquis [38] and by Tanaka et al. [39], the majority of the non-proportionality-induced additional hardening is quickly accumulated in the firsts cycles (in the considered case about 10–20).

5.2. Strain-controlled ratcheting experiments

5.2.1. Elastic and shear modulus

As for the zero-mean strain experiments, the cyclic evolution of E and G is analyzed for the uniaxial and multiaxial proportional ratcheting experiments plotting the mean elastic and shear moduli as a function of the equivalent accumulated plastic strain (see Fig. 9). To visualize the influence of ratcheting on the stiffness of the material, the corresponding LCF data are used as a reference. Fig. 9 shows only ratcheting data corresponding to the hysteresis loops antecedent to the reaching of the maximum strain level, after which the mean strain in axial direction no longer changes. For uniaxial and multiaxial experiments, only small differences between the elastic moduli under LCF and ratcheting conditions are observed. A larger but limited difference (up to 5%) is observed

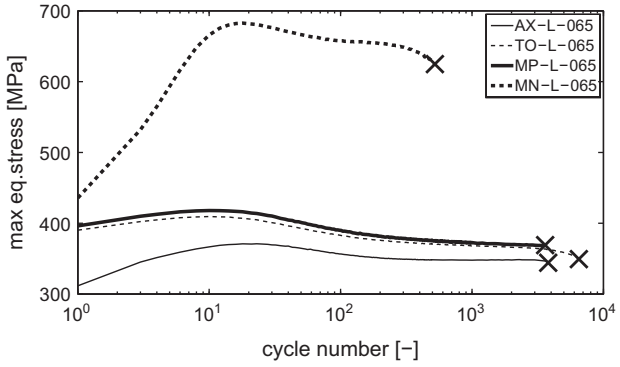

Fig. 8. Maximum equivalent stress versus number of cycles in uniaxial, torsional and multiaxial LCF experiments performed with an equivalent strain equivalent amplitude of 0.65%.

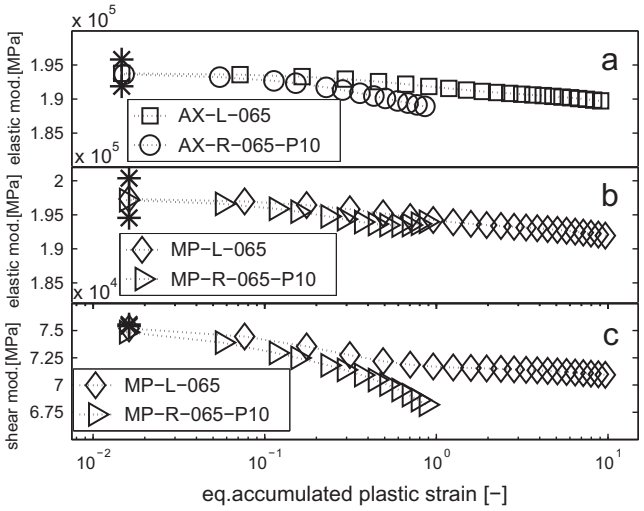

Fig. 9. Elastic modulus in uniaxial (a) and multiaxial proportional tests (b) and shear modulus in multiaxial proportional tests (c) versus equivalent accumulated plastic strain performed with an equivalent strain amplitude of 0.65%.

in the shear modulus for multiaxial proportional data. However, one cannot with certainty attribute this difference to the occurrance of ratcheting. As reported in [14] for uniaxial strain-controlled ratcheting experiments, depending on the exact loading conditions some buckling may occur, which can induce a deviation of the strain measured with the extensometer. By means of an elastic finite element simulation, one can demonstrate that the strain measurement error introduced by an axial misalignment of the specimen of only 0.05 mm, is sufficient to explain the deviation of the apparent stiffness reported in Fig. 9. A more precise determination of the effect of ratcheting on the stiffness of the material requires further testing.

5.2.2. Yield stress

As for the LCF experiments, the cyclic evolution of the equivalent yield stress is analyzed for ratcheting experiments adopting two threshold values for the definition of the proportionality limit. Fig. 10a and b report the yield stress values calculated using two different offset thresholds (0.025% and 0.0025%) for uniaxial tests. For multiaxial proportional tests the yield stresses with the two adopted offsets are computed considering both the axial and the shear stress contribution (e.g. $\sqrt{\sigma^2+3\tau^2}$) (see Fig. 10c and d). Fig. 10 only shows ratcheting data corresponding to the cycles

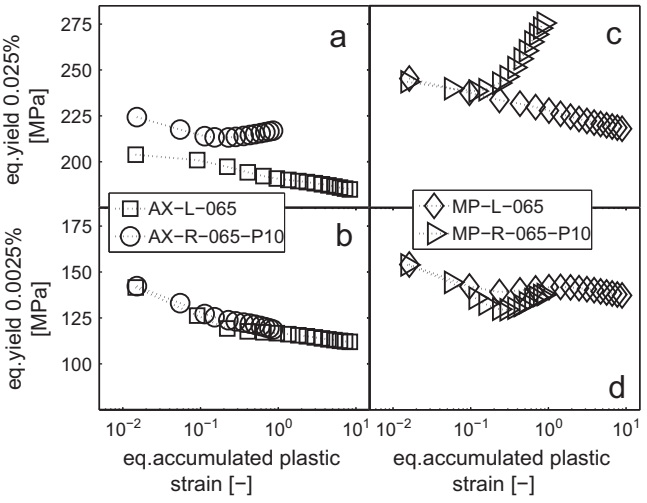

Fig. 10. Equivalent yield stress versus equivalent accumulated plastic strain in uniaxial (a, b) and multiaxial proportional experiments (c, d) performed with an equivalent strain amplitude of 0.65%.

antecedent to reaching the maximum axial strain level, after which the mean axial strain no longer changes. As reported in a previous work [14], treating uniaxial experiments, comparing the yield stress behavior calculated on the highest offset value with the corresponding LCF test, ratcheting affects the yield limit introducing an additional hardening. The same effect is reported also for multiaxial proportional experiments, in which the amount of accumulated additional hardening is qualitatively similar but consistently higher than the one noticed in axial test. On the other hand, when the lowest offset value (0.0025%) is used to analyze the same datasets, no significant evidences of ratcheting effects on the yield stress are observed. This finding underpins that when a constitutive model suitable for ratcheting is formulated and calibrated, the selection of the yield definition must be carefully evaluated.

In this case, the absence of the dependency of the yield stress on ratcheting when using the lower offset criterion, allows a more straightforward calibration of the model.

5.2.3. Cyclic hardening/softening

As for the LCF experiments, the cyclic evolution of the maximum equivalent stress for ratcheting tests performed with the same equivalent strain amplitude and ratcheting step is reported in Fig. 11. The graph only shows data corresponding to the cycles

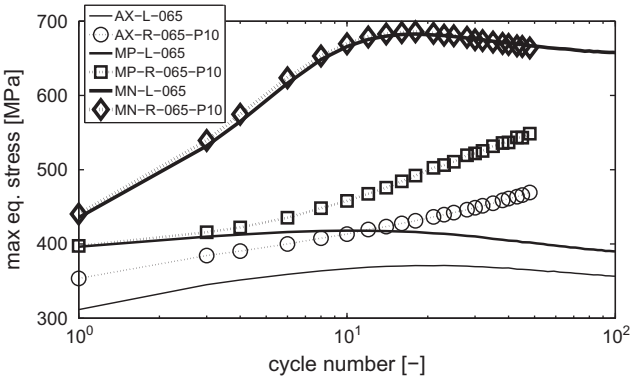

Fig. 11. Maximum equivalent stress versus number of cycles in uniaxial and multiaxial LCF and ratcheting experiments performed with an equivalent strain amplitude of 0.65%.

antecedent to reaching the maximum axial strain level. Comparing the maximum equivalent stress measured in uniaxial LCF and ratcheting experiments, one finds that the increment of the mean strain in axial direction introduces an additional hardening. The initial difference noticed between uniaxial experiments is due to the fact that these tests are carried out controlling the constant value of the cyclic deformation amplitude in engineering strain. Because of control-technical limits we were forced to use an engineering strain amplitude value that remains unchanged during an experiment. We opted to use a value which results in a true strain equivalent that is equal for the zero-mean-strain and the ratcheting experiments *during the constant mean strain phase of the experiment*, which represents the largest part of the fatigue life by far. Approximating the true strain ε_{true} with its logarithmic definition ε_{log} (see Eq. (12)), the engineering strain amplitude is calculated in order to have the intended true strain amplitude for a particular value of the mean strain (e.g. 5%).

$$\varepsilon_{true} \sim \varepsilon_{log} = ln(1 + \varepsilon_{eng}) \tag{12}$$

As a consequence of this, the strain amplitude during the initial cycles, i.e. the ratcheting phase, is not exactly equal for the zero-mean-strain and ratcheting experiments. It is higher than the one applied in the corresponding LCF test (0.68 instead of 0.65%) resulting in a harder stress response. A consistent ratcheting-induced hardening is found also analyzing the multiaxial proportional data. On the other hand, in non-proportional experiments the drifting of the mean strain in axial direction does not influence the stress response of the material.

In the case of ratcheting tests, the representation of the results by means of the maximum equivalent stress does not allow a complete understanding of the effect of ratcheting on the cyclic deformation behavior. A promising approach consists in analyzing the mean stress and the stress amplitude evolution instead of the maximum stress. Since it is not meaningful to retrieve the mean stress and the stress amplitude value in the equivalent space, the contributions of axial and shear stress components are analyzed separately evaluating their amplitude and mean values as a function of cycling. The cyclic evolution of the stress amplitude and mean stress in axial σ and shear direction τ are reported for ratcheting tests in Figs. 12 and 13. It is important to remark that, in the case of ratcheting, the stress range during loading differs significantly from the unloading one within one cycle. The definition of mean stress and of per-cycle stress amplitude must return a value that has to be consistent in case these features vary from cycle to cycle and that must not be sensitive to the ratcheting direction. The definition used here is the same adopted by Facheris and Janssens [14] considering a cycle as the sequence of a loading

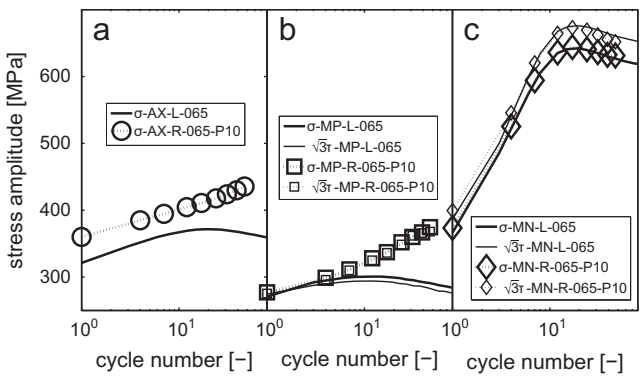

Fig. 12. Stress amplitude versus number of cycles in uniaxial (a), multiaxial proportional (b) and multiaxial non-proportional (c) LCF and ratcheting experiments performed with an equivalent strain amplitude of 0.65%.

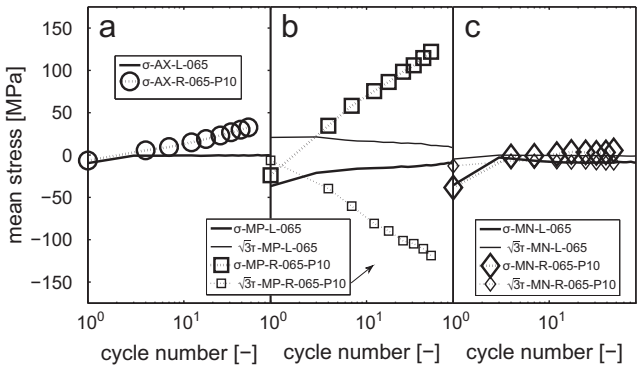

Fig. 13. Mean stress versus number of cycles in uniaxial (a), multiaxial proportional (b) and multiaxial non-proportional (c) LCF and ratcheting experiments performed with an equivalent strain amplitude of 0.65%.

and an unloading trait (or the reverse), computing the range and mean values using the extrema of each of these traits and calculating the per-cycle values as the average of the two traits. To allow an easier visualization of the influence of ratcheting on deformation response, the corresponding LCF data are also included for reference. A quantitative comparison of the two stress components is possible scaling the shear stress τ by a factor of $\sqrt{3}$.

In the uniaxial experiment, the drifting of the mean strain causes an increment of the stress amplitude (see Fig. 12a). A similar result is observed for multiaxial proportional tests (see Fig. 12b), in which the drifting of the mean strain in axial direction causes an additional hardening not only of the axial stress but also of the shear stress component. On the other hand, in non-proportional experiments (see Fig. 12c), the ratcheting does not affect the stress amplitude, neither for the axial nor for the shear component.

The drifting of the mean strain in axial direction is found to affect not only the evolution of the stress amplitude but also of the mean stress. While nearly no tension–compression asymmetry is found in uniaxial LCF experiments, ratcheting introduces a drifting of the mean stress having the same sign of the imposed mean strain (see Fig. 13a). In multiaxial proportional LCF data, the mean stress evolution (see Fig. 13b) shows a slight tension–compression asymmetry that slowly fades away during cycling. As for the uniaxial case, when ratcheting occurs, a drifting of the axial and shear mean stress is observed. In order to define the sign of this drifting, axial stress and strain are considered to be positive when a tension is applied. The definition of the sign for shear components is arbitrary, but considering that in proportional tests shear and axial strain histories are in phase, it is convenient to define the shear to be positive when a positive axial strain is applied. Using this convention and imposing a positive axial mean strain, the drifting of a mean stress observed in axial direction is positive and the one in shear direction is found to be negative. Finally, a completely different behavior is observed for multiaxial non-proportional experiments (see Fig. 13c) in which the continuous increment of the axial mean strain has no influence on the cyclic evolution of the mean stress neither in axial nor shear direction.

5.3. Ratcheting-induced contribution

The analysis of the stress amplitude evolution reveals that ratcheting introduces an additional hardening compared with LCF conditions. The procedure proposed by Facheris and Janssens [14] to quantitatively separate the hardening owing to ratcheting from the one owing to the cyclic hardening, is adopted in the current work. The first step of this methodology consists in

determining approximate curves describing the evolution of the stress amplitude for the considered dataset. The experimental curves are fitted by means of Eq. (13) which is a summation of exponential equations that are function of the equivalent accumulated plastic strain p and few constant parameters (i.e. α_i and β_i) that can be easily determined.

$$y = \sum_{i=1}^{n} \alpha_i \cdot e^{-\beta_i \cdot p} \tag{13}$$

These fitting curves allow a straightforward determination of the difference between the stress amplitude in a ratcheting and in a LCF test carried out with the same strain amplitude. This difference, equivalent to the ratcheting-induced additional hardening, is plotted against the value of the mean strain in axial direction (see Fig. 14a). If the vertical shift of the curves is attributed to the material heterogeneity and to experimental error, and only the slopes are considered, one can approximate the additional hardening to be linearly related to the axial mean strain for uniaxial and proportional tests, while no noticeable additional hardening is noticed for the non-proportional case. It is interesting to remark that the amount of additional hardening measured in the proportional test is very similar for the axial and the shear stress component and is larger than the one measured in uniaxial tests (e.g. a factor of 3).

The separation of cyclic and ratcheting-induced hardening contributions is also performed for the mean stress. Considering the tension–compression asymmetry effect to be negligible, this separation is a straightforward task and the whole mean stress drifting is considered to be a ratcheting effect. In Fig. 14b the mean stress is plotted versus the mean strain in axial direction. The ratcheting-induced mean stress evolution is qualitatively similar for uniaxial and proportional tests, but in the latter the measured values are considerably higher (e.g. a factor of 3). No noticeable effect of the drifting of the axial mean strain is noticed for the non-proportional case. This observation can be explained considering the fact that, as reported by Doong et al. [42], under non-proportional loading conditions the continuous change of the principal stress and strain directions promotes a stronger interaction between different slip systems compared to the proportional loading case. It is plausible that this interaction prevents the activation of the particular microstructural evolution mechanisms observed by Facheris et al. [43] under uniaxial ratcheting conditions. A very similar dislocation structure for specimens subjected to non-proportional LCF and ratcheting experiments would explain the nearly identical mechanical response noticed in the current work.

6. Fatigue endurance

6.1. Experimental fatigue behavior

In Fig. 15, an evaluation of the influence of the loading path on the life endurance reduction is presented for zero-mean strain LCF experiments. Comparing data corresponding to uniaxial and torsional LCF tests, it is evident that specimens systematically endure longer (a factor of 2) under torsion for all the considered equivalent strain amplitude levels. This result is in agreement with the observations of Socie [44], Kim et al. [45] and Chen et al. [46], who performed similar experiments on stainless steel grade AISI 304 at room temperature. They observed that the failure mode of this material depends on the stress state and on the applied cyclic strain amplitude. While under axial loading AISI 304 shows a normal fracture, under torsion it fails in shear mode in the low-cycle regime. Because of the irregularity of the shape of the crack surface, a mechanical interlocking occurs during pure shear loading causing the development of high frictional forces. The consequent reduction of the stress and strain field close to the crack tip is responsible for a lower crack growth rate in torsional tests. In multiaxial proportional LCF tests the simultaneous application of stress

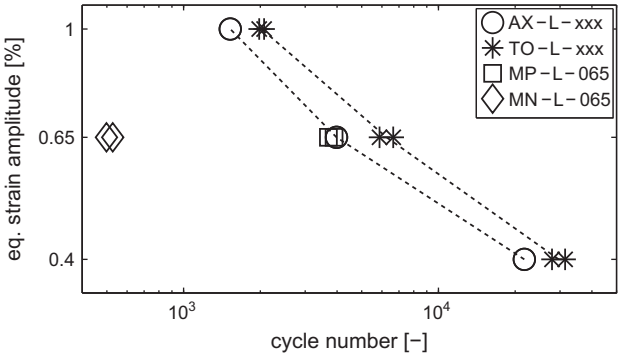

Fig. 15. Relationship between the imposed equivalent strain amplitude and number of cycles to failure for axial, torsional and multiaxial LCF experiments.

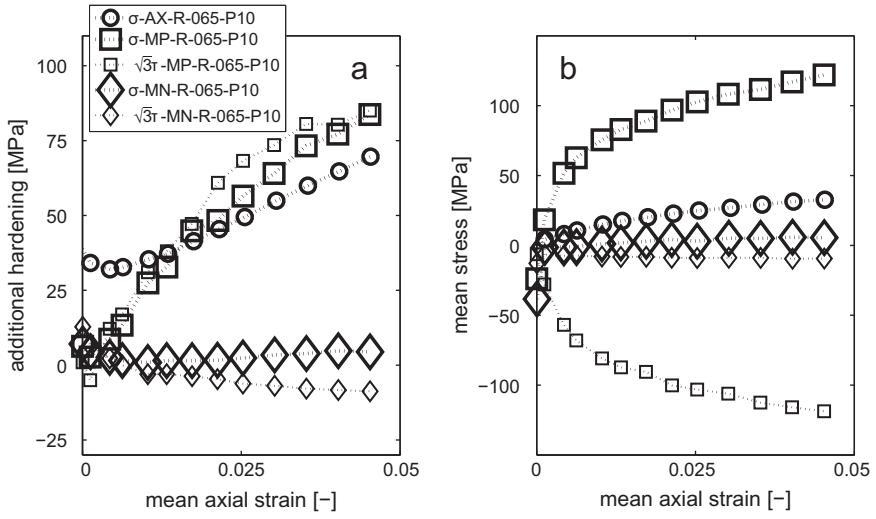

Fig. 14. Additional hardening (a) and mean stress (b) versus mean strain in axial direction for uniaxial and multiaxial ratcheting experiments performed with an equivalent strain amplitude of 0.65% and an axial ratcheting step of +0.1%/cyc.

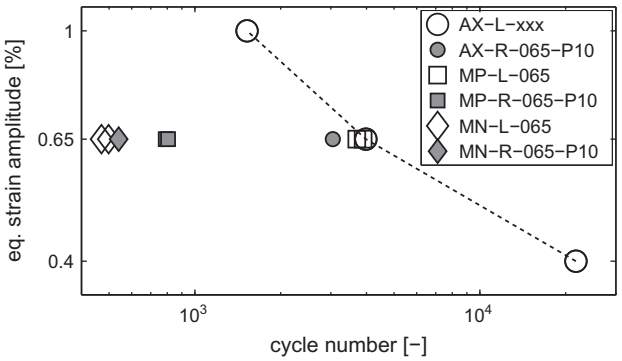

Fig. 16. Relationship between the imposed equivalent strain amplitude and number of cycles to failure for axial and multiaxial experiments.

and strain in a direction perpendicular to the crack reduces the friction forces and explains why in this case the observed fatigue life is comparable to the one measured in uniaxial experiments performed with the same equivalent strain amplitude. On the other hand, in the non-proportional LCF tests the fatigue life is substantially reduced (up to a factor of 10). This finding is in agreement with the work of Socie [44] who attributes the life reduction to the considerably harder material response induced by non-proportionality.

In Fig. 16, an evaluation of the influence of initial ratcheting on the life endurance reduction for uniaxial and multiaxial loading conditions is presented. In uniaxial ratcheting experiments a lower number of cycles to failure is noticed with respect to the corresponding LCF test (a factor of 2) suggesting that the ratcheting-induced additional hardening and the positive mean stress have a negative effect on the fatigue endurance [14]. The effect of ratcheting on the fatigue life reduction is found to be stronger (a factor of 5) in the case of multiaxial proportional loading. This observation is in agreement with the fact that the hardening behavior has a strong impact on the fatigue endurance. It is therefore logical to expect a stronger fatigue life reduction for multiaxial proportional experiments, in which the amount of ratcheting-induced additional hardening is considerably higher (a factor of 3) than in the corresponding uniaxial tests. The influence of (initial) ratcheting (followed by cyclic relaxation) on the fatigue life can change substantially considering different materials. The ratcheting influence will be particularly evident in materials like AISI 316L in which the loading sequence *'high to low'* plays an important role on the fatigue life [32]. Finally, the specimen subjected to multiaxial non-proportional ratcheting does not show any noticeable fatigue life reduction comparing with the corresponding LCF condition. This observation is in agreement with the fact that, for this class of experiments, the initial drifting of mean strain in axial direction does not influence the material response.

6.2. Fatigue life predictions

Providing as input the experimental stress and strain data, the three critical plane fatigue criteria previously described are used to assess the fatigue life of the specimens subjected to the prescribed loading conditions. The stresses and the strains are computed for planes with an angle of $0^\circ \leqslant \theta \leqslant 180^\circ$ from the axis of the specimen with an increment of 5°.

For the Smith–Watson–Topper and the Fatemi–Socie criteria, the fatigue parameters P_{SWT} and P_{FS} are evaluated for each loading cycle j in order to estimate the corresponding loss-of-life fraction $\frac{1}{N_f^j}$. The Palmgren–Miner [47,48] rule (see Eq. (14)) is then used to linearly sum the damage accumulated during the first 500 loading cycles.

$$C_{PM}(N) = \sum_{j=1}^{N} \frac{1}{N_f^j} \tag{14}$$

On the other hand, the Jiang criterion is an incremental damage model and does not require any cycle counting for general loading conditions. Knowing the evolution of $C_{PM}(N)$ or of $D(N)$ (for Jiang model) during the first 500 cycles and assuming the damage accumulation rate to be constant afterwards, it is straightforward to predict by means of a linear regression the number of cycles to failure for the investigated loading condition. The observed and predicted fatigue lives are summarized in Table 5. An evaluation of the performance of the considered fatigue criteria is available in Figs. 17–21, plotting the experimental fatigue lives versus the calculated ones for each damage model analyzed. The solid diagonal line signifies a perfect agreement between experiments and computations and the two dashed lines represent the twice error band.

Owing to the definition of the critical plane as the plane experiencing the maximum normal strain range, the SWT criterion provides acceptable fatigue life predictions for uniaxial LCF experiments showing a normal cracking mode failure (see Fig. 17). The

Table 5
Predicted and observed fatigue lives at room temperature. Reported in bold are the fatigue life predictions outside of the twice error band.

Test designation	Observed life	Predicted life				
		SWT	FS γ_{ampl}^{max}	FS P_{FS}^{max}	Jiang D^{max}	Jiang dD^{max}
AX-L-040	21,730	12,712	20,349	19,558	18,102	18,106
AX-L-065	3981	3351	4231	4749	5339	5340
AX-L-100	1524	1116	1131	1203	1289	1287
AX-R-065-P10	3048	2507	3643	3857	2232	2231
TO-L-040	31,400	**101,740**	23,222	24,791	20,829	17,629
TO-L-040	27,909	**107,610**	28,678	25,058	20,806	17,551
TO-L-065	5873	**12,281**	5156	6540	6983	5734
TO-L-065	6645	12,862	5143	6521	7674	6317
TO-L-100	2070	3479	2196	2240	2217	1756
TO-L-100	1980	3440	1598	1914	2149	1700
MP-L-065	3894	3657	3832	4047	3780	3775
MP-L-065	3700	3643	3951	4111	3573	3566
MP-R-065-P10	790	**2646**	**3215**	**2951**	1542	1523
MP-R-065-P10	795	**2819**	**3365**	**3080**	**1772**	**1756**
MN-L-065	527	**1292**	892	575	327	**241**
MN-L-065	470	**1276**	895	578	324	237
MN-R-065-P10	540	**1268**	921	582	316	**236**

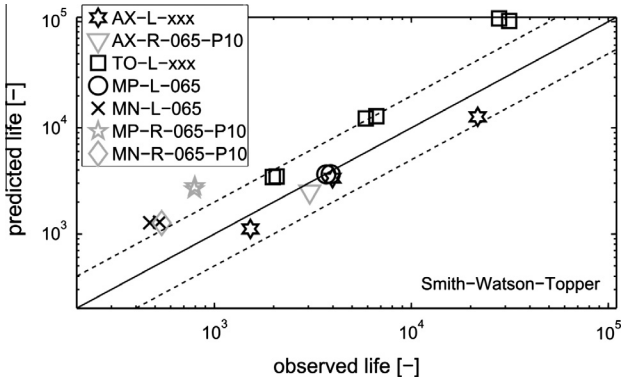

Fig. 17. Comparison of predicted and observed fatigue lives using the Smith–Watson–Topper damage criterion. The dashed lines define the twice error band.

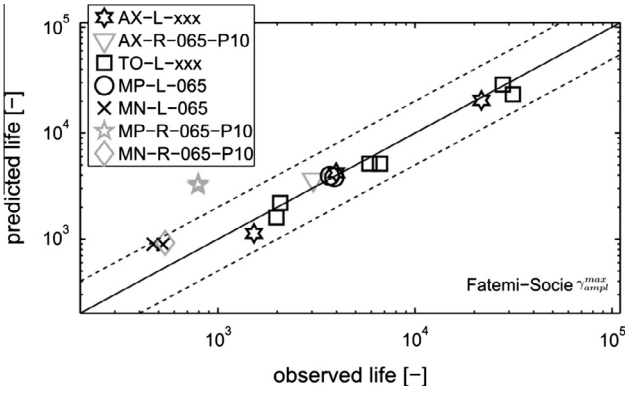

Fig. 18. Comparison of predicted and observed fatigue lives using the 'Fatemi–Socie γ_{ampl}^{max}' damage criterion. The dashed lines define the twice error band.

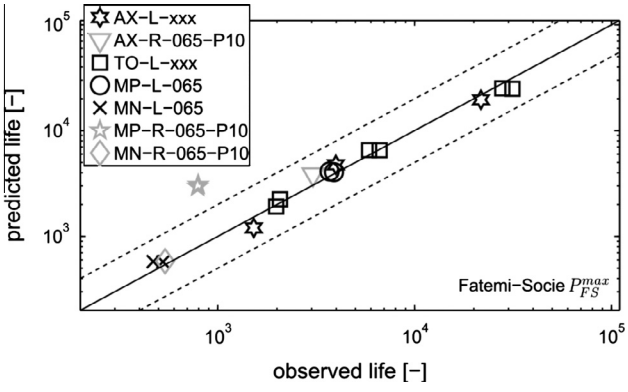

Fig. 19. Comparison of predicted and observed fatigue lives using the 'Fatemi–Socie P_{FS}^{max}' damage criterion. The dashed lines define the twice error band.

performance of the SWT model is also satisfactory for multiaxial proportional LCF tests characterized by negligible shear stress and strain on the critical plane. As expected, the accuracy of SWT model is poor under torsional loading conditions since in the LCF regime this class of materials nucleates cracks in shear mode [45,46]. In agreement with the work of Chen [46], the predictions for multiaxial non-proportional tests provided by SWT are strongly non-conservative because the fatigue criterion takes into account exclusively the effect of strain and stress in normal direction neglecting the important role played by shear stress and strain in the considered critical plane. The term $\sigma_{c,max}$ in Eq. (5) enables

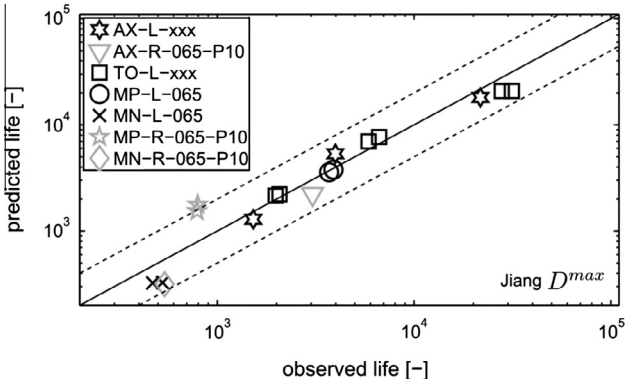

Fig. 20. Comparison of predicted and observed fatigue lives using the 'Jiang D^{max}' damage criterion. The dashed lines define the twice error band.

the SWT model to contemplate the effect of the ratcheting-induced additional hardening allowing an accurate reproduction of the consequent fatigue life reduction under uniaxial conditions. On the other hand, this information is not sufficient to provide precise predictions for the multiaxial proportional ratcheting case, because the significant contribution of the shear stress promoted by the mean strain drifting is neglected. An additional explanation for this overprediction is the utilization of the linear damage accumulation rule which does not allow to consider the 'high to low' loading sequence effect associated with the ratcheting-induced hardening observed in the first cycles. Consistently with the experimental results, no pejorative effect of ratcheting on the fatigue life is computed for the non-proportional loading case.

Thanks to the capability to take into account the role of the shear strain, the FS model provides a considerable improvement of the fatigue life predictions for torsional and multiaxial non-proportional LCF experiments with respect to the SWT criterion (see Figs. 18 and 19). In spite of the fact that the failure mode is predominantly normal, the performances of both versions of the FS criterion are acceptable for uniaxial and multiaxial proportional LCF conditions. While the fatigue life predictions provided by 'Fatemi–Socie P_{FS}^{max}' for the multiaxial non-proportional cases are extremely accurate (see Fig. 19), they are consistently non-conservative for the 'γ_{ampl}^{max}' version of the damage criterion (see Fig. 18). The cause of the error in the latter criterion lies in the fact that it determines the critical plane based solely on where the maximum value of the shear strain amplitude is found. Whereas in 'Fatemi–Socie P_{FS}^{max}' the critical plane is always perpendicular to the axis of the specimen, this is not true for the 'γ_{ampl}^{max}' version of the damage criterion. For multiaxial non-proportional loading, the material plane showing the maximum shear strain amplitude can be parallel or perpendicular to the specimen's axis. For the (parts of the) cycles in which the critical plane is found to be parallel to the axis of the sample, the corresponding stress in normal direction becomes very small, and so is the computed damage increment. As expected, neither of the versions of the FS criterion enhance the accuracy of the prediction for the loading case MP-R-065-P10 with respect to SWT. Part of the overprediction is again caused by the fact that the damage accumulation rule used in the FS criteria neglects the 'high to low' loading sequence effect associated with the ratcheting-induced hardening observed in the first cycles. In addition, one can argue that the information compressed in the variables $\gamma_{c,ampl}$ and $\sigma_{c,max}$ of Eq. (6) is not sufficient to completely describe the mechanical behavior induced by ratcheting in the critical plane.

A further enhancement is represented by the 'D^{max}' version of the Jiang fatigue criterion (see Fig. 20). This plastic work-based approach returns acceptable fatigue life predictions for all the

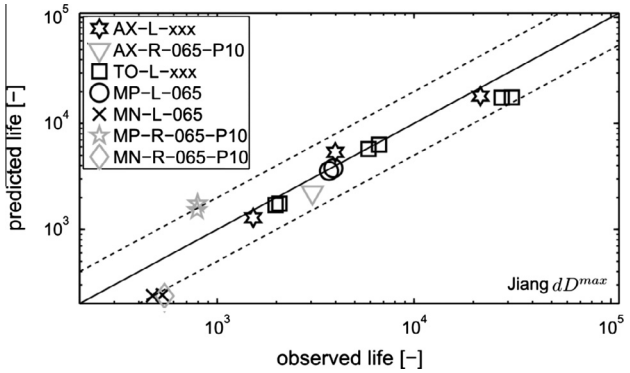

Fig. 21. Comparison of predicted and observed fatigue lives using the 'Jiang dD^{max}' damage criterion. The dashed lines define the twice error band.

loading conditions considered in the current work. Owing to its formulation, this model does not neglect any important stress or plastic strain contribution and at the same time has the capability to take into account the effect of the 'high to low' loading sequence on fatigue. As a consequence, the Jiang criterion shows an excellent accuracy also for particularly complex loading conditions as the ones occurring in the multiaxial proportional ratcheting case.

The performance of the 'dD^{max}' version of the Jiang criterion, adopting a different critical plane definition, is also investigated (see Fig. 21). As expected, defining the critical plane as the plane in which the damage accumulation increment dD is maximum, the Jiang model becomes more conservative. This observation is particularly evident for the loading cases characterized by a continuous changing of the critical plane during cycling (e.g. torsion and multiaxial non-proportional experiments).

7. Conclusions

Uniaxial, torsional and multiaxial LCF and strain-controlled ratcheting experiments have been carried out at room temperature on a AISI 316L plate material batch and the influence of strain amplitude, loading path and ratcheting on the cyclic deformation behavior has been investigated. Differently from the literature references concerning multiaxial experiments, controlling at the same both the axial and the torsional axes in strain, it was possible to perform a direct comparison of LCF and ratcheting data and to extrapolate the effect of the mean strain drifting on the material response.

The elastic and the shear modulus are observed to monotonically decrease during cycling in LCF tests, and the rate of this decrease is found to depend on the imposed equivalent strain amplitude. In addition, when a small enough offset value (e.g. 0.0025%) is adopted for its definition, the equivalent yield stress exhibits a monotonic decrease during cycling that is not particularly influenced by strain amplitude and ratcheting. Consistently with literature results, imposing the same equivalent strain amplitude, the maximum equivalent stress response evolution is similar for uniaxial, torsional and multiaxial proportional LCF tests. A considerably harder cyclic response is measured when a non-proportional loading history is prescribed justifying the huge reduction of fatigue life noticed in these tests. In uniaxial experiments, ratcheting is found to have an impact on the cyclic deformation behavior. The continuous increasing of the mean strain induces an additional hardening of the stress amplitude and a drifting of the mean stress. These ratcheting-induced differences in the cyclic deformation behavior explain the moderate fatigue life reduction measured in uniaxial experiments. Similar observations are also performed for multiaxial proportional tests, in which the drifting of mean strain in axial direction, influences also the shear stress component response. In addition, for this loading case, the effect of ratcheting on the mechanical response is found to be quantitatively stronger causing a more pronounced drop of fatigue life. On the other hand, ratcheting does not influence particularly neither the deformation response nor the fatigue life in non-proportional experiments.

Three critical plane fatigue criteria have been used to assess the fatigue lives of the specimens subjected to the investigated loading conditions. The Smith–Watson–Topper criterion provides acceptable fatigue life predictions for uniaxial and multiaxial proportional LCF tests but returns non-conservative calculations for the other loading cases, in which the contribution of shear stresses and strains on the critical plane is not negligible. A significant improvement is obtained with a shear strain-based approach such as the Fatemi–Socie model, providing a considerable enhancement of the accuracy of the fatigue life predictions for torsional and multiaxial non-proportional experiments. On the other hand, a poor performance was noticed under multiaxial proportional ratcheting conditions for both versions of the 'Fatemi–Socie' criterion. The observed overprediction is in part caused by the utilization of an elementary damage accumulation rule and in part by the impossibility to exhaustively consider the mechanical behavior promoted by ratcheting in the critical plane. Owing to his formulation, the Jiang model does not neglect any stress/strain contribution and takes into account the effect of the 'high to low' loading sequence. The implementation of these features allows this plastic work-based criterion to assess the number of cycles to failure with an acceptable accuracy for the limited number of experiments considered in the current work.

Acknowledgements

swissnuclear is acknowledged for funding through the PLiM project, in the context of which this work is performed. Prof. Edoardo Mazza is acknowledged for helping with his suggestions. Luca Signorelli is gratefully acknowledged for his invaluable support in test execution.

References

[1] Dahlberg MKF, et al. Development of a European procedure for assessment of high cycle thermal fatigue in light water reactors: final report of the NESC-thermal fatigue project. Technical report EUR 22763 EN, 2007.
[2] Igari T, Kobayashi M, Yoshida F, Imatani S, Inoue T. Inelastic analysis of new thermal ratchetting due to a moving temperature front. Int J Plasticity 2002;18:1191–217.
[3] Delobelle P. Synthesis of the elastoviscoplastic behavior and modelization of an austenitic stainless steel over a large temperature range, under uniaxial and biaxial loadings. Part I: Behavior. Int J Plasticity 1993;9:65–85.
[4] Hassan T, Kyriakides S. Ratcheting of cyclically hardening and softening materials: I. Uniaxial behavior. Int J Plasticity 1994;10:149–84.
[5] Kang G, Gao Q, Cai L, Yang X, Sun Y. Experimental study on uniaxial and multiaxial strain cyclic characteristics and ratcheting of 316L stainless steel. J Mater Sci Technol 2001;17:219–23.
[6] Feaugas X, Gaudin C. Ratchetting process in the stainless steel AISI 316L at 300 K: an experimental investigation. Int J Plasticity 2004;20:643–62.
[7] Taleb L. About the cyclic accumulation of the inelastic strain observed in metals subjected to cyclic stress control. Int J Plasticity 2013;43:1–19.
[8] Hassan T, Kyriakides S. Ratcheting of cyclically hardening and softening materials: II. Multiaxial behavior. Int J Plasticity 1994;10:185–212.
[9] Portier L, Calloch S, Marquis D, Geyer P. Ratchetting under tension–torsion loadings: experiments and modelling. Int J Plasticity 2000;16:303–35.
[10] Bocher L, Delobelle P, Robinet P, Feaugas X. Mechanical and microstructural investigations of an austenitic stainless steel under non-proportional loadings in tension–torsion-internal and external pressure. Int J Plasticity 2001;17:1491–530.
[11] Coffin Jr LF. The deformation and fracture of a ductile metal under superimposed cyclic and monotonic strain. Achiev High Fatigue Resist Metals Alloys, ASTM, STP 1970;467:53–76.
[12] Ohno N, Abdel-Karim M, Kobayashi M, Igari T. Ratchetting characteristics of 316FR steel at high temperature. Part I: Strain-controlled ratchetting experiments and simulations. Int J Plasticity 1998;14:355–72.

[13] Mizuno M, Mima Y, Abdel-Karim M, Ohno N. Uniaxial ratchetting of 316FR steel at room temperature. Part I: Experiments. Eng Mater Trans ASME 2000;122:29–34.
[14] Facheris G, Janssens KGF. Cyclic mechanical behavior of 316L: uniaxial LCF and strain-controlled ratcheting tests. Nucl Eng Des 2013;257:100–8.
[15] Karolczuk A, Macha E. A review of critical plane orientations in multiaxial fatigue failure criteria of metallic materials. Int J Fracture 2005;134:267–304.
[16] Smith KN, Topper TH, Watson P. A stress–strain function for the fatigue of metals (stress–strain function for metal fatigue including mean stress effect). J Mater 1970;5:767–78.
[17] Fatemi A, Socie DF. A critical plane approach to multiaxial fatigue damage including out-of-phase loading. Fatigue Fract Eng M 1988;11:149–65.
[18] Glinka G, Shen G, Plumtree A. A multiaxial fatigue strain energy density parameter related to the critical fracture plane. Fatigue Fract Eng M 1995;18:37–46.
[19] Liu KC, Wang JA. An energy method for predicting fatigue life, crack orientation, and crack growth under multiaxial loading condition. Int J Fatigue 2001;23:129–34.
[20] Jiang Y. A fatigue criterion for general multiaxial loading. Fatigue Fract Eng M 2000;23:19–32.
[21] Ince A, Glinka G. A modification of Morrow and Smith–Watson–Topper mean stress correction models. Fatigue Fract Eng M 2011;34:854–67.
[22] Ince A, Glinka G. A generalized fatigue damage parameter for multiaxial fatigue life prediction under proportional and non-proportional loadings. Int J Fatigue 2013;62:34–41.
[23] Liu Y, Mahadevan S. A unified multiaxial fatigue damage model for isotropic and anisotropic materials. Int J Fatigue 2007;29:347–59.
[24] Youtsos AG, Gutierrez E, Verzeletti G. Viscoplastic behavior of stainless-steel AISI 316L under cyclic loading conditions. Acta Mech 1990;84:109–25.
[25] ASTM, ASTM E606/E606M – 12, Standard test method for strain-controlled fatigue testing. In: ASTM international, West Conshohocken (PA USA): Book of Standards Volume 03.01; 2012.
[26] ASTM, ASTM E2207 – 08, Standard practice for strain-controlled axial-torsional fatigue testing with thin-walled tubular specimens. In: ASTM International, West Conshohocken (PA, USA): Book of Standards Volume 03.01; 2008.
[27] Coffin JLF. A study of the effects of cyclic thermal stresses on a ductile metal. Trans ASME 1954;76:931–50.
[28] Manson SS. NACA Rep. TN-2933, 1953.
[29] Chopra OK, Shack WJ. Review of the margins for ASME code fatigue design curve-effects of surface roughness and material variability. Tech. Rep. NUREG/CR-6815 ANL-02/39, Washington (DC, USA): Division of Engineering Technology, Office of Nuclear Regulatory Research, U.S. Nuclear Regulatory Commission; 2003.
[30] Janssens KGF, Niffenegger M, Reichlin K. A computational fatigue analysis of cyclic thermal shock in notched specimens. Nucl Eng Des 2009;239:36–44.
[31] Socie DF, Marquis GB, editors. Multiaxial fatigue. Warrendale (PA): Society of Automotive Engineers; 2000. p. 212.
[32] Wong YK, Hu XZ, Norton MP. Plastically elastically dominant fatigue interaction in 316L stainless steel and 6061-T6 aluminium alloy. Fatigue Fract Eng M 2002;25:201–13.
[33] Polák J, Fardoun F, Degallaix S. Analysis of the hysteresis loop in stainless steels I, Austenitic and ferritic steels. Mat Sci Eng A-Struct 2001;297:144–53.
[34] Jiang Y, Zhang J. Benchmark experiments and characteristic cyclic plasticity deformation. Int J Plasticity 2008;24:1481–515.
[35] Alain R, Violan P, Mendez J. Low cycle fatigue behavior in vacuum of a 316L type austenitic stainless steel between 20 and 600 °C. Part I: Fatigue resistance and cyclic behavior. Mater Sci Eng 1997;229:87–94.
[36] Polák J, Obrtlík K, Hájek M. Cyclic plasticity in type 316L austenitic stainless-steel. Fatigue Fract Eng M 1994;17:773–82.
[37] Benallal A, Legallo P, Marquis D. An experimental investigation of cyclic hardening of 316-stainless steel and of 2024-aluminum alloy under multiaxial loadings. Nucl Eng Des 1989;114:345–53.
[38] Benallal A, Marquis D. Constitutive-equations for nonproportional cyclic elastoviscoplasticity. J Eng Mater-Trans ASME 1987;109:326–36.
[39] Tanaka E, Murakami S, Ooka M. Effects of plastic strain amplitudes on nonproportional cyclic plasticity. Acta Mech 1985;57:167–82.
[40] Chaboche JL. Time-independent constitutive theories for cyclic plasticity. Int J Plasticity 1986;2:149–88.
[41] Facheris G, Janssens KGF. An internal variable dependent constitutive cyclic plastic material description including ratcheting calibrated for AISI 316L. Comp Mater Sci 2014;87:160–71.
[42] Doong SH, Socie DF, Robertson IM. Dislocation substructures and nonproportional hardening. J Eng Mater-Trans ASME 1990;112:456–64.
[43] Facheris G, Pham MS, Janssens KGF, Holdsworth SR. Microscopic analysis of the influence of ratcheting on the evolution of dislocation structures observed in AISI 316L stainless steel during low cycle fatigue. Mat Sci Eng A-Struct 2013;587:1–11.
[44] Socie DF. Multiaxial fatigue damage models. J Eng Mater-Trans ASME 1987;109:293–8.
[45] Kim KS, Lee BL, Park JC. Biaxial fatigue of stainless steel 304 under irregular loading. Am Soc Test Mater 2000;1389:79–93.
[46] Chen X, Jin D, Kim KS. A weight function-critical plane approach for low-cycle fatigue under variable amplitude multiaxial loading. Fatigue Fract Eng M 2006;29:331–9.
[47] Palmgren A. Die Lebensdauer von Kugellagern. Zeitschrift des Vereins Deutscher Ingenieure 1924;68:339–41.
[48] Miner MA. Cumulative damage in fatigue. J Appl Mech 1945;12:159–64.